Interaction of SrO-terminated $SrTiO_3$ Surface with Oxygen, Carbon Dioxide, and Water

Aleksandar Staykov,[a,*] Shun Fukumori,[b] Kazunari Yoshizawa,[b]
Kenta Sato,[c] Tatsumi Ishihara,[a,c] John Kilner[a,d]

[a)] International Institute for Carbon Neutral Energy Research, Kyushu University, Japan

[b)] Institute for Materials Chemistry and Engineering, Kyushu University, Japan

[c)] Applied Chemistry Department, Kyushu University, Japan

[d)] Materials Science Department, Imperial College London, UK

Abstract

The interaction of SrO terminated $SrTiO_3$ surface with molecular carbon dioxide and water has been investigated using first-principle theoretical methods and surface analysis techniques. We have studied the formation of a surface $SrCO_3$ layer and various possible products of H_2O interaction with the SrO surface, such as, surface chemisorbed water and the formation of a surface hydroxide layer. The co-adsorption of CO_2 and H_2O was explained both theoretically and experimentally showing that its products follow a complex temperature dependence and as a result, the surface composition may vary between carbonate and surface chemisorbed water. Our theoretical simulations have shown that the presence of water molecules in the gas phase might assist the molecular oxygen / lattice oxygen exchange reaction by stabilization of the surface oxo species in the transition state with a hydrogen bond mechanism. As a result, the activation barrier for molecular oxygen dissociation is decreased leading to an increase in the surface exchange rate constant. Our study demonstrates that the SrO terminated $SrTiO_3$ surface is not static but instead, dynamically responds to external factors such as gas composition, humidity, and temperature. As a result, the surface phases can show different trends for the surface exchange reaction with molecular oxygen by either an increase or decrease in the exchange rate.

Introduction

In recent years, the advance of carbon neutral energy technologies has been a driving force for the active research in energy related materials for applications in fuel cells,[1] solar cells,[2] artificial photosynthesis devices,[3-7] high capacity Li-ion batteries,[8] etc. Amongst those technologies, particular interest has been devoted to solid oxide fuel cells (SOFC) due to their remarkable ability to operate with various fuels, i.e., hydrogen, methane, methanol, as electricity generating devices (fuel cells) or as fuel generating devices (electrolyzers).[1] Thus, when coupled with a fluctuating renewable energy source, e.g., solar cells, wind turbines, etc., and a fuel storage facility, the SOFC can smooth out the fluctuations, operating either as an energy storage device through energy conversion into chemical fuel or as a steady power generating device, using the accumulated chemical fuel as required.

An SOFC comprises of a fuel electrode, a solid oxide electrolyte, and an air electrode where the fuel oxidation, oxide ion transport, and oxygen reduction reaction take part, respectively. To increase the mobility of the oxide ions and to facilitate the oxygen reduction reaction without the use of precious metal catalysts, SOFCs operate at elevated temperatures (600℃-1000℃).[1] Complex oxides with the perovskite lattice (perovskites) and alternating layered perovskite and rock salt lattices (Ruddlesden-Popper phase) are often employed in SOFCs due to their good oxide ion conductivity and surface exchange coefficient between molecular oxygen and lattice oxygen.[1, 9-16] Perovskites are layered oxides of two or more cations with different ionic radii and a general formula of ABO_3. In the perovskite lattice, the smaller cation (B-site) occupies the center of an octahedron with oxide ions at its apices while the larger cation (A-site) occupies the 12-coordinated voids in the lattice between the octahedra. The ionic radii ratio between the A-site cations and B-site cations is important for the perovskite lattice stability and the physical and chemical properties.[17] It is worth noting that while the original perovskite mineral is $CaTiO_3$ and many perovskites are oxides of two or more metal cations, the crystallographic perovskite lattice is not limited to metal oxides and perovskite ordering can be observed in various materials such as the hybrid organic/inorganic perovskites which recently find application in the field of solar cells.[18]

Owing to their small ionic radii, transition metals usually occupy the B-sites at the perovskite lattices of complex metal oxides, while A-sites are occupied by larger alkaline, earth-

alkaline, or rare earth metallic cations. While most perovskites with the general formula of ABO_3 will have some oxygen vacancies, usually their concentration is rather low to achieve reasonable oxide ion conductivity.[14, 19] Thus, various doping elements can be introduced into the perovskite lattice which can promote the formation of oxygen vacancies and further enhance the ionic conductivity. For example, iron doping in $SrTiO_3$ lattice can lead to elimination of one oxide ion per two Fe^{3+} ions in the lattice.[20] Doping can be performed either on the A-sites, B-sites, or both, A- and B-sites, and can lead to perovskite materials with complicated chemical composition and various tunable properties such as electronic conductivity, ionic conductivity, or surface exchange.

Understanding the correct surface and near surface composition of perovskite materials is crucial for their application as air electrodes in SOFCs. A typical ABO_3 perovskite can be cleaved in various possible crystallographic planes. Thus, understanding the proper surface termination requires understanding of the surface reconstruction processes under operating conditions.[19] The perovskites are ionic layered materials and their surfaces obey the Tasker principles for stability of ionic solid/gas interface.[21] The surface reconstruction strongly depends on the charge compensation in the layers. Perovskites with non-polar surfaces such as $SrTiO_3$ show surface with similar composition to the corresponding bulk while polar surfaces, e.g., $KTaO_3$ show significant reconstruction with several layers significantly deviating from the bulk stoichiometry.[19] A recent experimental study has pointed out that perovskite oxide surfaces always show the AO-surface termination when exposed to elevated temperatures in high P_{O2} ambient, even for short time.[22] As a result, the catalytically active transition metals on the B-site are buried in the subsurface layer while the A-site elements are exposed at the solid/gas interface. We have shown that the catalytic activity of the AO-terminated perovskite surfaces strongly depends on the presence of surface oxygen vacancies which expose the electronic states of the BO_2-sublattice to the gas/solid interface.[23] This is especially true for perovskite lattices with alkaline and earth alkaline metals on the A-site, e.g., Sr, Ba, etc., while different catalytic mechanism based on d-electron occupancy was proposed for perovskites with rare earth elements on the A-site, e.g., La, Pr, etc.[24] The electronic properties in the vicinity of surface oxygen vacancies of $SrTiO_3$ have shown that those vacancies are not simply spatial voids but are regions in space characterized with high electron density.[20] As the molecular oxygen activation and dissociation in an electrophilic reaction, surface oxygen vacancies would be the preferred surface active sites. The oxygen vacancies in $SrTiO_3$ have been found to be slightly stabilized within the SrO surface layer compared to the subsurface

TiO_2 layer.[23] In addition, the oxygen vacancies on the SrO surface of $SrTiO_3$ show tendency to pair due to electronic relaxation in the vicinity of the vacancy pair.[23]

SOFCs operate in air rather than high-purity oxygen and the gas composition on the air electrode includes a gas mixture that contains N_2, CO_2, H_2O, SO_x, NO_x, etc., beside O_2. That gas composition would vary depending on the environmental factors and the geographic location of the device, i.e., in the vicinity of large industrial plants might lead to higher concentration of SO_x, pollution of big cities would lead to higher concentration of CO_2, tropical or costal climate would increase the air humidity. Thus, besides the oxygen reduction reaction, various other processes can take place on the air electrodes in different environmental conditions, either under operating conditions or during the exposure of the electrodes to air after their preparation. As a result of those processes, secondary phases can be formed on the electrode surface which can either enhance or degrade the electrode operation. Amongst those phases the most important are the formation of surface carbonates, surface hydroxides, and physisorption or chemisorption of water molecules.[25-27] A knowledge of the real surface composition of ABO_3 perovskite air electrodes for solid oxide devices is crucial for the understanding of the chemical activity on the electrode surface and for the further optimization of electrode performance. Theoretical studies on surface termination of perovskites have so far been limited to the chemical composition of the investigated materials.[19] Various experimental techniques, such as LEIS, can provide information about the chemistry of the outermost surface layer, however, so far, the experimental studies were performed after treatment in high-purity oxygen, and not equivalent to operating conditions.[22] Under pure oxygen the surface termination would be the AO-termination. Those AO-terminated perovskite surfaces might differ significantly from the surface terminations in air, which would be a result of the chemical interaction between the AO-terminated surfaces and the components of the air. It is important to investigate the possible chemical reactions of the AO-terminated perovskite with some major constituents of air and also with combinations of those constituents in order to determine possible synergistic effects. This will allow us to predict the chemical composition of perovskite surfaces as a function of the composition of the atmosphere to which those materials are exposed.

The SOFC electrodes operate at elevated temperatures, 600°C -1000°C while various surface analysis measurements are performed on electrode materials under ambient conditions, i.e. ~25°C. Temperature is an important factor that can determine the stability of different chemical

phases on the electrode surfaces by shifting the equilibrium of the relevant reaction. Thus, it is possible for the surface termination to be different at 25°C and 1000°C in ambient air. While the temperature is not included directly in the first-principle calculations, we can evaluate the effect of the temperature on a given chemical reaction by estimating the reaction activation barrier. Chemical reactions characterized with high activation barriers would be possible only at elevated temperatures while chemical reactions with a low activation barrier would proceed at lower temperature. In this work the term high temperature refers to SOFC operating conditions of 600°C -1000°C while low temperature refers to normal conditions of 25 °C.

In this paper we investigate the surface adsorption of H_2O and CO_2 (or mixture of both) on SrO terminated $SrTiO_3$ surface. We study the formation of surface carbonates and hydroxides as well as their influence on the oxygen reduction reaction. Strontium titanite, $SrTiO_3$, and iron doped strontium titanite, $SrTi_xFe_{1-x}O_3$, are examples of ABO_3 perovskites with simple, well-defined stoichiometry and well-understood elemental composition and defect chemistry. While $SrTiO_3$ is a wide band-gap semiconductor and is characterized with low oxygen vacancy concentration, $SrTi_xFe_{1-x}O_3$ is characterized with electrical conductivity and larger number of oxygen vacancies that can be controlled with the Fe/Ti ratio. Neither of those two materials has been directly applied in commercial SOFC systems due to the widespread application of other perovskites with superior electronic and ionic conductivity such as $La_xSr_{1-x}CoO_3$, $La_xSr_{1-x}Ga_yMg_{1-y}O_3$, etc., however, $SrTi_xFe_{1-x}O_3$ is actively used in the SOFC research as a model material for air electrode of SOFCs. $SrTi_xFe_{1-x}O_3$ is also used to investigate space-charge layers caused by surface termination and defect distribution that could arise in more complex perovskites. $SrTi_xFe_{1-x}O_3$ is used as a material with tunable Fermi level in Fermi-level engineered devices. Most importantly, the SrO terminated $SrTi_xFe_{1-x}O_3$ surface is used as a realistic model system for SrO terminated perovskite materials ($La_xSr_{1-x}CoO_3$, $La_xSr_{1-x}Ga_yMg_{1-y}O_3$, etc.) used as air electrodes in commercial SOFCs. SrO terminated surfaces in perovskite air electrodes tend to build secondary phase precipitations of Sr-nanoparticles, SrO-rocksalt layers, carbonates and hydroxides. Our study will provide model on how SrO-terminated surfaces of ABO_3 perovskites interact with common components of the air such as H_2O and CO_2. In addition, we will provide guidelines on those interactions at SOFC operating conditions and at ambient temperature (at which many common experimental measurements are performed, i.e. TEM, STM, LEIS, etc.).

Methods of investigation

Theoretical calculations

Periodic, plane wave DFT calculations and first principle molecular dynamics were performed with the Vienna Ab initio Software Package (VASP).[28-31] The Perdew–Burke–Ernzerhof (PBE) exchange-correlation functional was applied using projector augmented wave pseudopotentials. Electron energies were converged to 10^{-5} eV using the tetrahedron smearing method with Bloch correction for bulk systems and Gaussian smearing for surfaces. The calculations were performed with 400 eV cut-off energy and Monkhorst-Pack k-points mesh of 6 × 6 × 4 for the bulk systems and 6 × 6 × 1 for the slab systems. Geometry optimization was performed using the conjugated gradient algorithm. For bulk systems relaxation was performed of the cell volume, cell shape, and atomic positions. For slab models, relaxation was performed for the atomic positions only. Slabs were constructed using 8 alternating layers of SrO and TiO_2 in the [0 0 1] crystallographic directions. The coordinates of the atoms in the bottom four layers (two SrO and two TiO_2) were fixed, while the coordinates of the four layers (two SrO and two TiO_2) at each surface were fully relaxed. The relaxation was performed until the forces converged to values bellow 0.03 eV/Å^2. Whilst DFT calculations provide excellent agreement with the experiment for metallic systems, as well as, very good trend for the geometry and reactivity of metal oxides and molecular systems, it is well known that the method fails to describe correctly the optical properties of semiconductors and insulators due to underestimating of the energy levels of the conduction band. This problem could be avoided by the use of the GGA+U method, which takes into account local correlations within selected orbitals. However, the results depend on the value of the on-site Coulomb interaction, as well as, on the set of orbitals for which the corrections are applied. The value of U is selected to match an experimentally observed property, most often the band gap. Such an approach introduces an empirical term to DFT and thus it deviates significantly from its first principle nature. A better approach (completely based on first principle methods) would be the use of hybrid DFT functional, which includes a degree of Hartree-Fock mixing. However, hybrid DFT calculations with plane wave basis sets and large unit cells are computationally expensive. That is why in this study we have employed the GGA+U approach for the d-orbitals of Ti. The value of U for Ti was estimated to be 8.0 eV by reproducing the optical band gap of $SrTiO_3$, 3.2 eV, and comparing with data from the literature.[32-33] Vibrational frequency calculations require

well converged electron density. That is why in our study the frequency calculations were performed for electron density, which was converged to energy of 10^{-7} eV. Activation barriers for various reaction mechanisms were obtained using the nudged elastic band method (NEB) combined with the climbing nudged elastic band method (cNEB). In the process of NEB calculations five images were used between the starting and ending geometries. Starting geometries for the surface species were obtained using the computational annealing technique with first-principle molecular dynamics. The annealing was performed for 500 fs with time step of 0.5 fs, starting temperature of 1000 K and final temperature of 300 K. Throughout this study, we have used the graphical visualization package VESTA.[34] We have analyzed the reaction rates using the Arrhenius equation. For similar reactions, we have assumed that the preexponential factor is the same and we have ignored its contribution to the reaction rate constant. We should note that this is a strong approximation and it was applied with care only to compare rates of similar reactions at similar conditions.

$$k = Ae^{-\frac{E_a}{RT}} \quad (1)$$

In equation 1 *A* denotes the preexponential factor, *Ea* is the activation barrier obtained from the NEB calculations, R is the gas constant, and *T* is the reaction temperature. The preexponential factor contains information for the collision probability between the participating species.

In our work we have performed surface coverage estimation based on the Langmuir theory. We have assumed defect-free, atomically flat $SrTiO_3$ surface with SrO- termination and surface lattice oxygens as the surface active adsorption sites. We have studied the competitive coadsorption of H_2O and CO_2, as well as the adsorption of each of those species in the absence of the other, for various concentrations and temperatures. According to Langmuir theory the surface coverage is given with the following equation:

$$\theta_x = \frac{K_x P_x}{1 + K_x P_x} \quad (2)$$

In equation 2, θ_x denotes the surface sites occupied by x (x is either CO_2 or H_2O), K_x (capital K) denotes the equilibrium constant for the adsorption/desorption process of x, P_x denotes the partial pressure of x. The equilibrium constant is calculated as follows:

$$K = \frac{k^{ads}}{k^{des}} \tag{3}$$

In equation 3 k^{ads} is the rate constant of the adsorption reaction and k^{des} is the rate constant of the desorption reaction, calculated with equation 1 using activation energies estimates with DFT.

To create a model which studies the competitive coadsorption of CO_2 and H_2O we assume that the $SrTiO_3$ surface is initially pre-coved with H_2O molecules. This assumption is justified from our results and matches the purpose of our study to demonstrate that H_2O can mitigate surface carbonate formation on $SrTiO_3$ surface. We assume three possible processes on the surface: CO_2 displaces H_2O / CO_2 desorbs; H_2O adsorbs on a free site / H_2O desorbs; CO_2 adsorbs on a free site / CO_2 desorbs. The equilibrium constants of the three processes are denoted with K'_{CO2}, K_{H2O}, *and* K_{CO2}, respectively. The surface coverage for the CO_2 molecules is given with the following equation:

$$\theta_{CO2} = \frac{K'_{CO2}P_{CO2}}{1 + K'_{CO2}P_{CO2} + K_{H2O}P_{H2O}} + \left(1 - \frac{K'_{CO2}P_{CO2}}{1 + K'_{CO2}P_{CO2} + K_{H2O}P_{H2O}} - \frac{K_{H2O}P_{H2O}}{1 + K'_{CO2}P_{CO2} + K_{H2O}P_{H2O}}\right) \left(\frac{K_{CO2}P_{CO2}}{1 + K_{CO2}P_{CO2} + K_{H2O}P_{H2O}}\right) \tag{4}$$

The surface coverage for the H_2O molecules is given with the following equation:

$$\theta_{H2O} = \frac{K_{H2O}P_{H2O}}{1 + K'_{CO2}P_{CO2} + K_{H2O}P_{H2O}} \tag{5}$$

The first part of the sum in equation 4 represents the CO_2 occupied sites which are result of CO_2 replacing H_2O in equilibrium with CO_2 desorption from those sites. The second part of the sum in equation 4 is a product of the surface free sites (difference between all available sites and the sites occupied by CO_2 replacing H_2O and the sites occupied by H_2O) and the sites occupied by CO_2 direct adsorption on free surface sites in competition with H_2O. Namely, the second term of

the sum in equation 4 accounts for the direct competition for free surface adsorption sites between CO_2 and H_2O.

Experimental procedure

In-situ FTIR analyses were performed using a diffused reflectance measurement cell with a CaF_2 single-crystal window, while a KBr single-crystal window was used for *in-situ* FTIR analysis of CO_2 adsorption with and without H_2O. Approximately 30 mg of the sample powder was placed in the cell prior to acquiring spectra, heated at 500 °C for 2 h under vacuum, then cooled to room temperature. Spectra were recorded with a JASCO 610 spectrometer (JASCO, Japan) coupled with a Hg-Cd-Te semiconductor (MCT) detector. Background spectra were acquired prior to introducing CO_2 gas and these were subtracted from subsequent sample spectra recorded at a 4 cm^{-1} resolution for each spectrum. After CO_2 was introduced (0.13 atm), the sample was heated at each temperature for 1 h. When wet CO_2 was exposed to $SrTiO_3$ sample, 2.8 vol% humidity was added to dry CO_2.

Results and discussion

Our calculations start with the interaction of the CO_2 molecule and the H_2O molecule with the SrO-terminated $SrTiO_3$ surface. The results are summarized in Figure 1. Both molecules are characterized by a barrierless interaction with the surface. The absence of a transition state suggests that those reactions proceed rapidly, and the gas molecules have surface sticking coefficients close to one. The CO_2 molecule is activated by a decrease in the O-C-O angle from 180° to 126°. The interaction of CO_2 with the SrO-terminated surface results in the formation of a surface $SrCO_3$ monolayer. The initial geometry of CO_3^{2-} on the SrO terminated SrTiO3 surface was taken form the work of Sopiha et al.[25] Bader population analysis shows that the carbonate ion has charge close to 2- compensating the 2+ charge of Sr in the surface layer. The C-O bond length is 1.38 Å and the Sr-O (from the CO_2 molecule) distance is 2.57 Å. The CO_3^{2-} is tilted with respect to the surface.

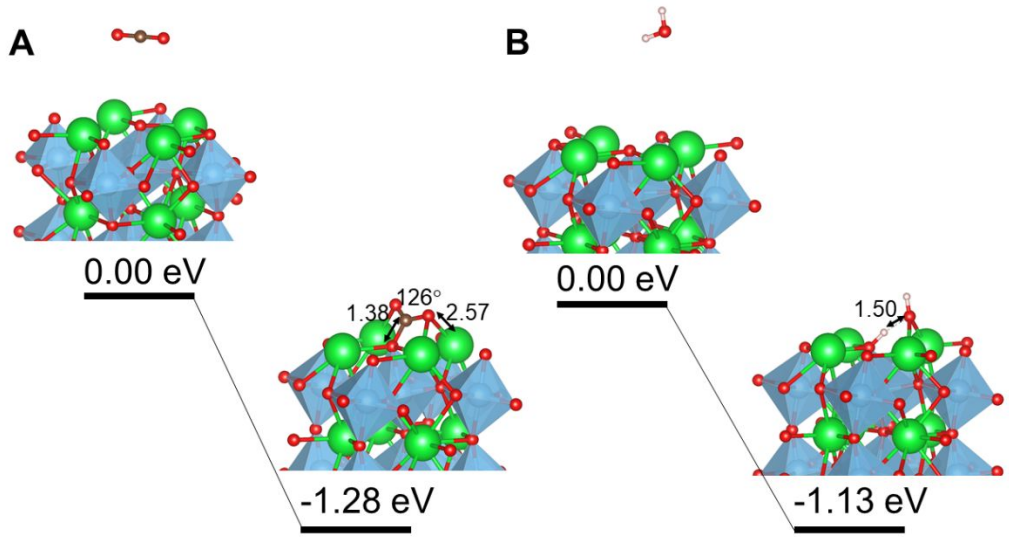


Figure 1. Interaction of gas molecules with SrO-terminated $SrTiO_3$ surface. A: Interaction of CO_2; B: Interaction of H_2O. For simplicity of the representation, only the three outermost layers of $SrTiO_3$ are shown. Bond lengths are given in Å.

The formation of carbonate layer on $SrTiO_3$ surface was recently investigated with theoretical methods by Sopiha et al.[25] In their study, they have shown that the carbonate layer significantly alters the electronic properties of the $SrTiO_3$ surface by increasing the surface band gap. The effect has been observed on both TiO_2 and SrO terminated surfaces.[25] While it is generally believed that surface carbonate precipitation would have negative effect on the oxygen exchange properties of perovskites due to an isolating overlayer, a recent paper proposes a mechanism resulting in enhanced oxygen exchange, assisted by $SrCO_3$ precipitations.[27] Such enhance surface exchange would be a result of mismatch between the perovskite and carbonate lattices leading to cracks that expose B-site elements to the solid gas interface.[27]

Water chemisorbs on the SrO-terminated surface as it dissociates into an H-atom and an OH species. The H-atom binds to a surface oxide ion while the OH species binds at a bridge site between two surface Sr ions. The initial geometry of H_2O chemisorbed on the SrO terminated $SrRuO_3$ surface was taken form the work of Halwidl et al.[35] and in our calculations was adopted to the $SrTiO_3$ surface. The H-atom and the OH group form a hydrogen bond with an H-O distance of 1.5 Å. The interaction of CO_2 with the surface is exothermic by 1.28 eV and the interaction of

H_2O with the surface is exothermic by 1.13 eV. Water interaction with SrO terminated perovskite surfaces has been extensively investigated experimentally and theoretically. The surface chemisorbed water molecules were reported for SrO terminated $SrRuO_3$ by Halwidl et al.[35] They have shown a chemisorption structure similar to the one estimated in our work using first principle simulations and STM measurements. They have also demonstrated a rotational motion of the chemisorbed water molecules over the perovskite surface. The stability of surface water on Ti-rich $SrTiO_3$ surfaces has been discussed by Baccera-Toledo et al.[36] Water adsorption and dissociation on $SrTiO_3$ and $SrZrO_3$ surface has been studied with DFT methods by Evarestov et al.[37]

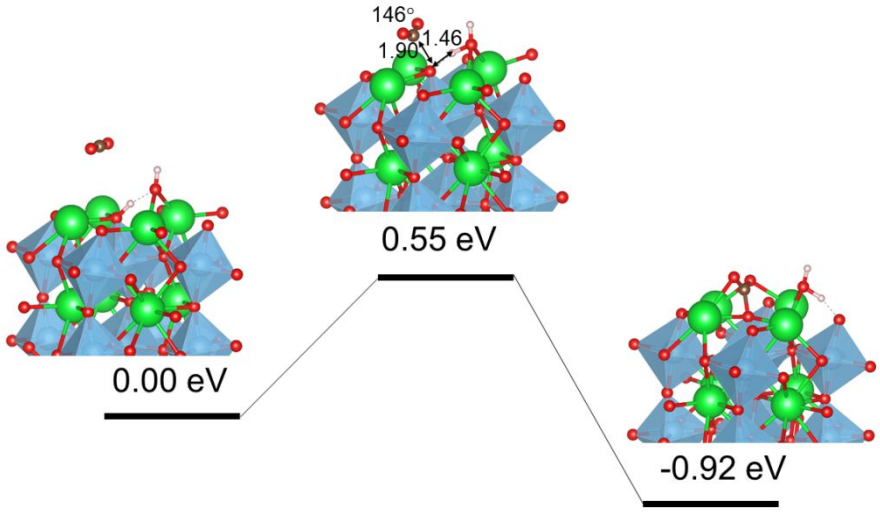


Figure 2. Interaction of CO_2 with wet SrO-terminated $SrTiO_3$ surface. For simplicity of the representation, only the three outermost layers of $SrTiO_3$ are shown. Bond lengths are given in Å.

To elucidate the effect of the operating gas humidity on the $SrCO_3$ formation we investigate CO_2 interaction with an SrO-terminated surface with pre-adsorbed water. The results are summarized in Figure 2. Calculations start with surface partially covered by chemisorbed H_2O molecules, i.e. dissociated water with a hydrogen bond between the H-atom and OH group. In the transition state geometry, the CO_2 molecule is bent to 146° and the surface water molecule is recombined as CO_2 repels the H-atom away from its site over the surface oxide ion. In the transition state geometry, the distance between the surface oxide ion and the CO_2 molecule is 1.90 Å. The

distance between the surface oxide ion and the water molecule is 1.46 Å. Finally, surface carbonate is formed, and the water molecule is repelled to a neighboring surface site. The reaction is exothermic by 0.92 eV and activation barrier of 0.55 eV. Thus, to replace the water molecule from the surface, the CO_2 molecule would require significant energy. If the preexponential factor in the Arrhenius equation is ignored, then the rate constant for the carbonate formation at 25°C and surface with chemisorbed water would correspond to 6 x 10^{-4}. The rate constant for the same reaction at 800°C would correspond to 2 x 10^{-3}. From the results in Figure 1 and Figure 2 we can conclude that no increase of the temperature is required to form a surface carbonate layer on the dry $SrTiO_3$ surface. At high temperatures this carbonate layer will decompose, and CO_2 will desorb from the surface. However, in case of wet $SrTiO_3$ surface, the carbonate will not be formed at low temperatures. At elevated temperature, water will be replaced by CO_2. In conclusion, high humidity would have beneficial effect to prevent the formation of surface $SrCO_3$ phase.

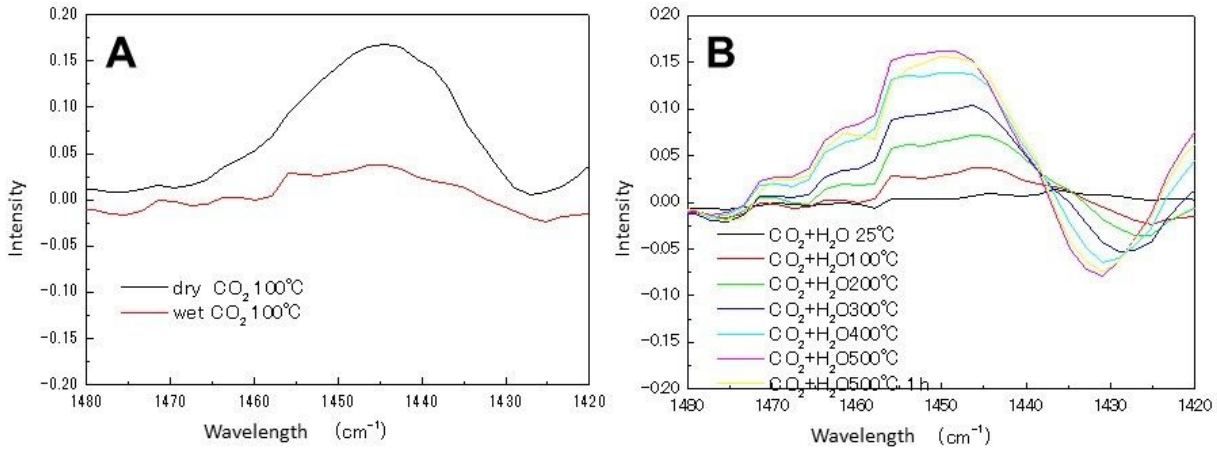


Figure 3. IR spectra of $SrTiO_3$ surface after interaction with CO_2 gas. A: IR spectra of $SrTiO_3$ surface after interaction with dry and wet CO_2 gas; B: Temperature dependence of the IR spectra of $SrTiO_3$ surface after interaction with wet CO_2 gas.

To verify our theoretical simulations, we measure the IR spectra of $SrTiO_3$ surface in the presence of dry and wet CO_2. We are monitoring the characteristic peak of the CO_3^{2-} group at 1450 cm^{-1}. The comparison between $SrTiO_3$ interaction with wet and dry CO_2 is shown in Figure 3 A. In case of dry CO_2, the characteristic peak of the carbonate is observed, however, in case of wet

CO_2 no peak was found at 100℃. This result verifies that at low temperature the gas humidity can prevent the formation of surface carbonates. We have further investigated the temperature dependence of the interaction of wet CO_2 with $SrTiO_3$ in the interval of 25℃ - 500℃. The results are summarized in Figure 3 B. At low temperature (25℃ and 100℃) there is no peak at 1450 cm^{-1}. With the increase of the temperature, the peak at 1450 cm^{-1} gradually increases its intensity and reaches the maximum corresponding to the peak for dry CO_2 gas at 500℃. The experimental IR spectra support the theoretical findings that at low temperature humidified CO_2 would not form surface carbonate layer and the surface will be dominated by chemisorbed water molecules. In contrast, dry CO_2 will lead to carbonate formation which will cover the perovskite surface. At elevated temperature the mitigation effect of the water molecules will be reduced, and it will completely disappear at 500℃. For that temperature the surface will be carbonate dominated.

Table 1. Calculated vibrational frequency modes of bulk $SrTiO_3$ unit cell, bulk $SrCO_3$ unit cell, $SrTiO_3$ slab terminated with half monolayer of $SrCO_3$, and $SrTiO_3$ slab terminated with monolayer of $SrCO_3$. Only the ten highest frequencies are given for each model. All values are in cm^{-1}. Red color highlights the vibration modes compared in Figure 4.

$SrTiO_3$ bulk	$SrCO_3$ bulk	$SrTiO_3$ slab half layer $SrCO_3$	$SrTiO_3$ slab monolayer $SrCO_3$
771.48	1583.43	1602.42	1661.38
746.46	1486.61	1273.31	1657.95
704.55	1486.57	961.88	1275.90
590.14	1479.37	835.00	1235.99
578.86	1472.71	747.94	972.06
578.30	1471.69	735.38	892.34
573.37	1446.86	705.67	805.79
564.13	1429.00	688.22	804.37
557.92	1095.74	650.50	740.46
540.35	1094.47	627.87	720.86

To elucidate the origin of the IR peak in Figure 3 we have performed vibrational frequency calculations of bulk $SrTiO_3$ unit cell, bulk $SrCO_3$ unit cell, $SrTiO_3$ slab terminated with half monolayer of $SrCO_3$, and $SrTiO_3$ slab terminated with monolayer of $SrCO_3$. The four spectra are compared in Table 1. Our calculations show that $SrTiO_3$ does not have vibrational frequencies above 1000 cm^{-1}. The frequencies above 1000 cm^{-1} which were computed in the spectra of bulk $SrCO_3$ unit cell, $SrTiO_3$ slab terminated with half monolayer of $SrCO_3$, and $SrTiO_3$ slab terminated with monolayer of $SrCO_3$ should be a result from the vibrations of the carbon atom within the carbonate group. However, significant difference was observed in the spectra of the bulk $SrCO_3$, and the spectra of $SrTiO_3$ slabs terminated with half and with one monolayer of $SrCO_3$. When we compare the computed spectra in Table 1 with the experimental spectrum in Figure 3 we can conclude that the experimental peak is not a result of any of the vibrations characteristic for $SrTiO_3$ which are below 1000 cm^{-1}, and that the experimental peak at 1450 cm^{-1} corresponds to vibration of the bulk $SrCO_3$. The peak at 1450 cm^{-1} is absent in the computed spectra of the half monolayer of $SrCO_3$ and one monolayer of $SrCO_3$ covering the $SrTiO_3$ slab. To further elucidate the origin of the IR peaks we compare in Figure 4 the vibration of bulk $SrCO_3$ at 1446 cm^{-1} with the vibrations of half monolayer $SrCO_3$ covering of the $SrTiO_3$ slab at 1602 cm^{-1} and 1273 cm^{-1}. The values are highlighted with red color in Table 1.

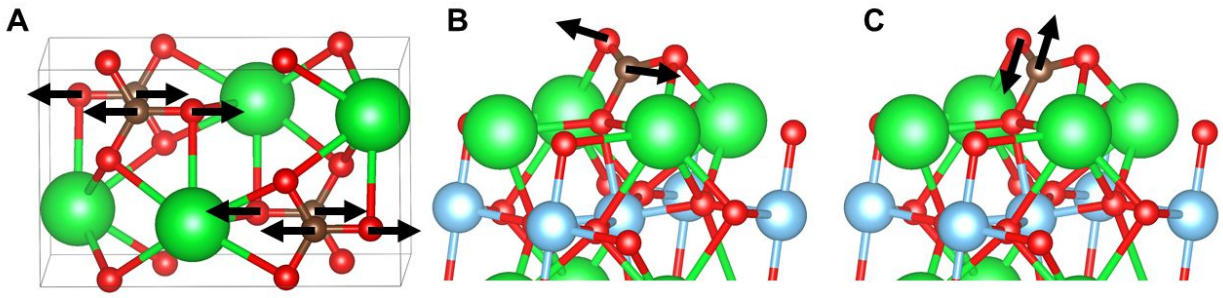


Figure 4. Visualization of calculated vibration frequencies for bulk $SrCO_3$ and half monolayer $SrCO_3$ covering of the $SrTiO_3$ slab. A: vibration of bulk $SrCO_3$ at 1446 cm^{-1}; B: vibrations of half monolayer $SrCO_3$ covering of the $SrTiO_3$ slab at 1602 cm^{-1}; C: vibrations of half monolayer $SrCO_3$ covering of the $SrTiO_3$ slab at 1273 cm^{-1}.

Figure 4 demonstrates that vibrations in bulk $SrCO_3$ and half monolayer $SrCO_3$ covering of the $SrTiO_3$ slab have different origin. The bulk $SrCO_3$ vibration at 1446 cm^{-1} is a result of synchronous symmetrical vibration of two C-O bonds. Owing to the very different geometry of the half monolayer $SrCO_3$ covering of the $SrTiO_3$ slab such vibration is geometrically impossible and thus, it is not observed. On the $SrCO_3$ surface two possible C-O vibrations were observed: at 1602 cm^{-1} parallel to the surface and at 1273 cm^{-1} perpendicular to the surface. Our theoretical and experimental IR spectra provide a hint that a thick, bulk-like phase of $SrCO_3$ was formed over the $SrTiO_3$ surface as a result of the interaction with the dry CO_2. This carbonate phase is either a result of several nanometer thick $SrCO_3$ surface precipitation or due to the formation of large $SrCO_3$ nanoparticles at the regions where the grain boundaries reach the oxide surface and provide channels for Sr^{2+} segregation.

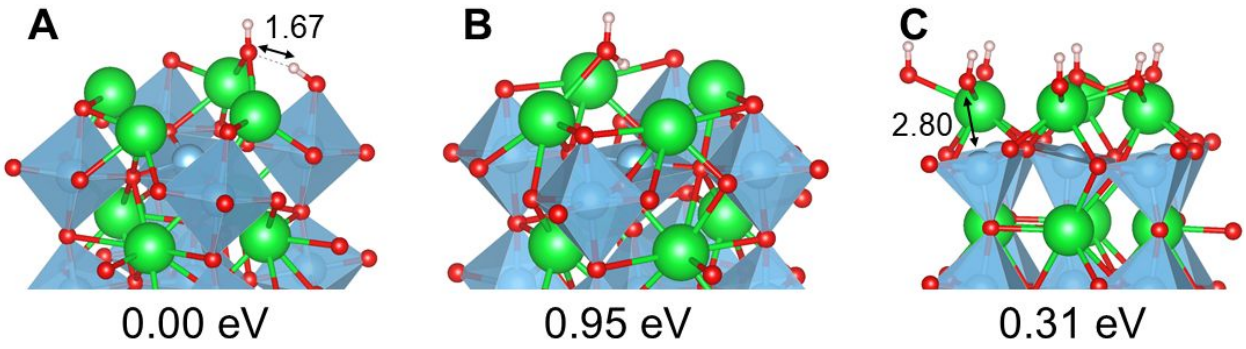


Figure 5. Interaction of H_2O with a SrO-terminated $SrTiO_3$ surface with a surface oxygen vacancy. Three possible geometries were investigated. A: H_2O chemisorbed next to the vacancy site; B: H_2O physiosorbed in the vacancy site; C: dissociated water molecule with OH group occupying the vacancy site and H atom on the remaining surface oxygen. For simplicity of the representation, only the three outermost layers of $SrTiO_3$ are shown. Bond lengths are given in Å.

Perovskites naturally possess a small population of oxygen vacancies, however, as mentioned above, doping at either of the A or B-site cations can further increase the oxygen vacancy concentration. Oxygen vacancies are slightly more stabilized within the surface SrO layer[20, 23] and they play an important role in the catalytic activity of a SrO-terminated surface where they are the active sites for oxygen reduction reaction and sites for oxygen incorporation in the

oxide lattice.[20, 23] In this work we investigate the interaction of molecular water with a surface oxygen vacancy site. The results are summarized in Figure 5. In Figure 5, the central surface oxygen atom is missing. We compare the relative energies of a water molecule which is chemisorbed next to the vacancy site (Figure 5 A), a water molecule which is physiosorbed in the vacancy site (Figure 5 B), and a dissociated water molecule with the OH group occupying the vacancy site and the H atom on the remaining surface oxygen (Figure 5 C). Comparing the relative energies, the most stable surface structure is the chemisorbed water on a site neighboring the oxygen vacancy. The least stable geometry is the water molecule physiosorbed in a surface oxygen vacancy site which is 0.95 eV greater in energy compared to the chemisorbed water geometry. The dissociated water molecule with OH group occupying the vacancy site and H atom on the remaining surface oxygen has relative energy of 0.31 eV greater than the chemisorbed water geometry. It is worth noting the geometry of the dissociated water molecule with OH group occupying the vacancy site and H atom on the remaining surface oxygen. In this case the SrO-terminated surface transformed to a $SrOH^+$ terminated surface. The O-atoms left their position in the $SrTiO_3$ lattice and formed a surface OH layer, i.e., surface hydroxide. The relative energy of 0.31 eV suggests that surface hydroxide layer will be formed at moderate temperatures.

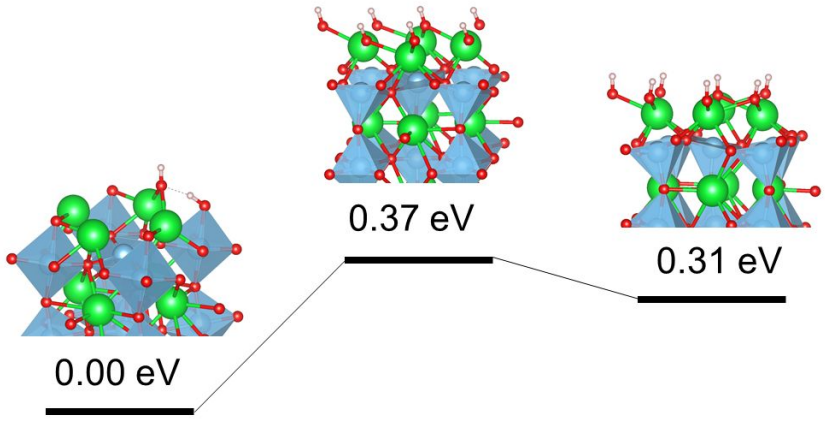


Figure 6. H_2O dissociation on SrO-terminated $SrTiO_3$ surface with surface oxygen vacancy. For simplicity of the representation, only the three outermost layers of $SrTiO_3$ are shown.

We have investigated the activation barrier for water dissociation on the $SrTiO_3$ surface with a surface oxygen vacancy. The results of the simulation are summarized in Figure 6. The

water molecule is dissociated, and the result is a $SrOH^+$ surface layer. The activation barrier is 0.37 eV and the reaction is endothermic by 0.31 eV. The activation barrier for the reverse reaction, i.e., formation of surface chemisorbed water, is 0.06 eV and it is an exothermic reaction. It is an important conclusion that surface oxygen vacancies are not the preferred surface sites for water adsorption and thus, surface water would not poison the catalytically active sites for oxygen reduction reaction.[23] As a result, the increased humidity of the operating gas in SOFC would not have negative effect on the device operation. However, a positive effect might be observed due to suppressed formation of a surface carbonate layer. Nevertheless, theoreticians and experimentalists should consider the correct surface composition and termination in the presence of CO_2 and H_2O.

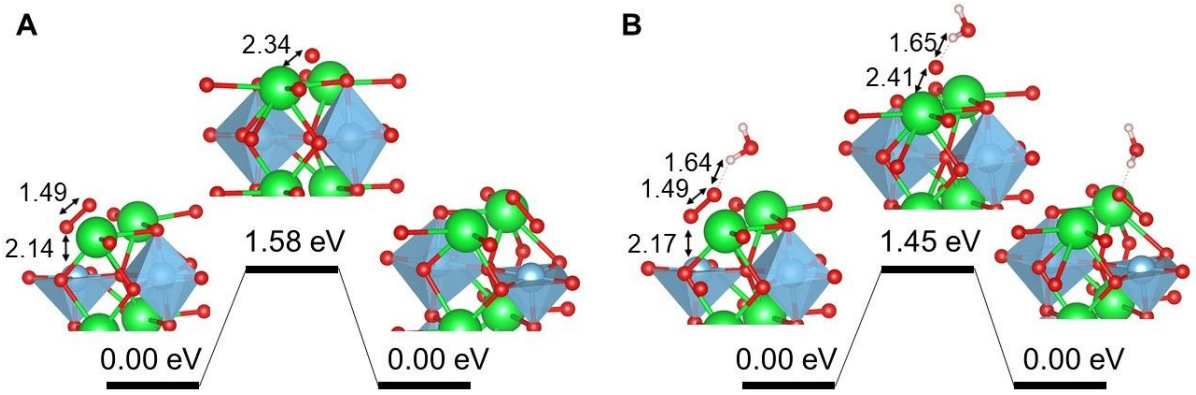


Figure 7. Oxygen exchange reaction on n-doped on SrO-terminated $SrTiO_{2.875}$ surface. A: reaction over dry surface; B: water assisted reaction. Bond lengths are given in Å.

To elucidate further the effect of gas phase water on perovskite electrodes performance, we investigate the oxygen surface exchange reaction with dry and wet oxygen gas. In a recent study we have shown and oxygen exchange on an SrO terminated surface of $SrTiO_3$ is catalyzed through electron density transfer from the surface oxygen vacancy site. In this study we investigate $SrTiO_3$ slab model with a single oxygen vacancy in the surface layer and a stoichiometry $SrTiO_{2.875}$. The defective SrO-terminated perovskite surface offers more possibilities for adsorption sites than the pristine SrO-terminated perovskite surface. In this work we investigate single oxygen vacancy defect on the surface. Such structures have been extensively studied in the literature and here we

follow our previous calculations which include both DFT and DFT-MD simulations.[20,23] Our previous results demonstrate that oxygen vacancies are stabilized within the SrO surface layer of $SrTiO_3$.[23] The structure of O_2 molecule on the defective SrO-terminated surface has been estimated in Ref. 23 so we used that structure as initial geometry in our simulations. Molecular oxygen is chemisorbed within the vacancy site with O-O bond elongated to 1.49 Å. Such an O-O distance corresponds to an activated oxygen molecule in its peroxo state. The distance between the Ti-atom at the vacancy site and the oxygen molecule is 2.14 Å. It was shown that oxygen dissociation proceeds through a transition state over a Sr-Sr bridge site.[23] Once the oxygen molecule is dissociated, one of the oxygen atoms is incorporated in the perovskite lattice while the second atom can flip back to restore the original oxygen molecule or recombine with neighboring lattice oxygen to form a cross molecule, i.e. a molecule with one oxygen atom originating from the gas phase and one oxygen atom originating from the solid phase.[23] In this case, in an isotopic oxygen exchange experiment with $^{18}O_2$ gas, "cross" molecules of $^{18}O^{16}O$ should be observed to form. In Figure 7 A we have estimated the activation barrier for this reaction to be 1.58 eV. In the transition state geometry, the distance between the surface oxo-species and the nearest Sr-atom is 2.34 Å. The high activation barrier corresponds to a high-temperature process which is the case for SOFC devices in operation.

In second simulation we have placed a water molecule in the vicinity of the chemisorbed oxygen molecule. It was reported that water has positive effect on the oxygen exchange reaction on perovskite electrodes of fuel cells.[38] We should note that the in our simulation the water molecule is part of the gas and is only weakly physiosorbed on top of a surface Sr-atom instead of chemisorbed as shown in Figure 1 B. Such geometry would correspond to water molecule from the gas phase close to the surface. In the relaxed geometry one hydrogen atom of the water molecule is pointing towards an oxygen atom from the activated oxygen molecule. The H-O distance is 1.64 Å which corresponds to the distance of a hydrogen bond. The O-O bond remains 1.49 Å as in the case with dry surface. The distance between Ti-atom at the vacancy site and the oxygen molecule is 2.17 Å. Similar transition state to the dry surface is estimated (Figure 7 B) with oxygen atom at a Sr-Sr bridge site. In the transition state geometry, the surface water molecule rotates and keeps the hydrogen bond with the dissociated oxygen atom. The H-O distance remains 1.65 Å. the distance between the surface oxo-species and the nearest Sr-atom is 2.41 Å. Finally, the "cross" molecule is formed between the oxygen atom from the original oxygen molecule and

a lattice oxygen. In the final geometry the surface water molecule is oriented in such a way that it prevents the O-H hydrogen bond.

The estimated activation barrier for the formation of a "cross" molecule assured by the operating gas humidity is 1.45 eV. Our results show that for the wet gas the activation barrier for oxygen exchange is decreased by 0.13 eV compared to the dry gas. The reason is in the stabilization of the transition state through water molecule facilitated hydrogen bond. For the dry gas, the dissociated oxygen atom located over a Sr-Sr bridge is highly unstable due to almost no electron transfer from both Sr-atoms. However, for the wet gas, electron density is transferred through the hydrogen bond, which reduces the overall energy of the transition state. If we use the values of the activation energies calculate in Figure 7 A and Figure 7 B in the Arrhenius equation and we ignore the effect of the preexponential factor, A, assuming that the both systems are very similar, then the rate constant for oxygen exchange on dry surface will be 3.79×10^{-8} while the rate constant for the exchange reaction assisted by water would be 1.55×10^{-7}. The ratio between the rate constant for the wet gas versus the rate constant on dry gas would be 4. This simple calculation was performed for a temperature of 800℃ and it demonstrates the beneficial effect of water on the surface oxygen exchange reaction.

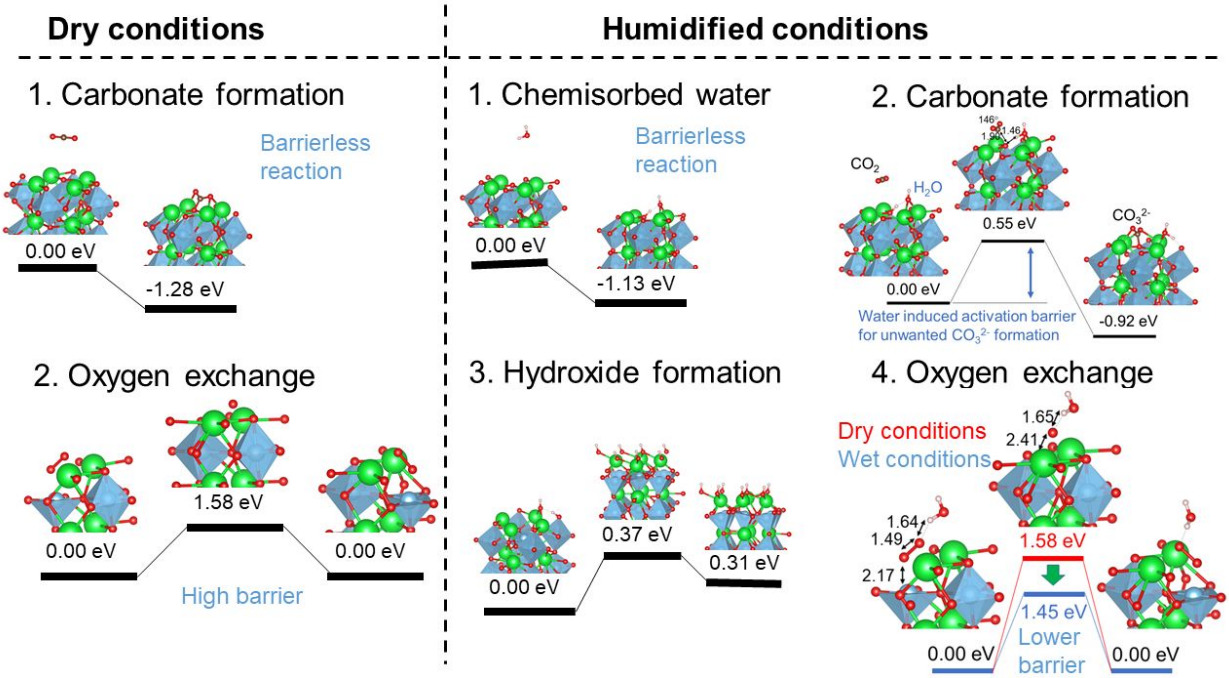


Figure 8. Overview of the investigated processes on dry and humidified SrO-terminated $SrTiO_3$ surfaces. Bond lengths are given in Å.

Figure 8 summarizes the possible processes investigated with first-principle methods on dry and humidified SrO-terminated $SrTiO_3$ surfaces. On the dry surface, $SrCO_3$ is formed without an activation barrier. The oxygen exchange reaction occurs with a high activation barrier. On the humidified surface, a chemisorbed water layer is formed without an activation barrier. $SrCO_3$ is formed with an activation barrier of 0.55 eV. Surface hydroxide is formed from the chemisorbed water layer with an activation barrier of 0.37 eV. The activation barrier for the oxygen exchange reaction is lower compared to the dry surface. Depending on the operating atmosphere different processes will be observed on the electrode surface.[39]

We have used the analytical model summarized in equations 2-5 to estimate qualitatively the surface coverage on the defect-free $SrTiO_3$ surface in presence of CO_2 and H_2O for various temperatures, P_{H2O}, and P_{CO2}. To estimate K_{H2O}, and K_{CO2}, K'_{CO2}, respectively, we have used the results from our DFT simulations. K_{H2O} is calculated with activation of 0.0 eV for water adsorption and 1.13 eV for water desorption. K_{CO2} is calculated with activation of 0.0 eV for CO_2 adsorption and 1.28 eV for CO_2 desorption. K'_{CO2} is calculated with activation of 0.55 eV for CO_2 displacing water and 1.47 eV for CO_2 desorption displaced by water. The result of our analysis is presented in Figure 9.

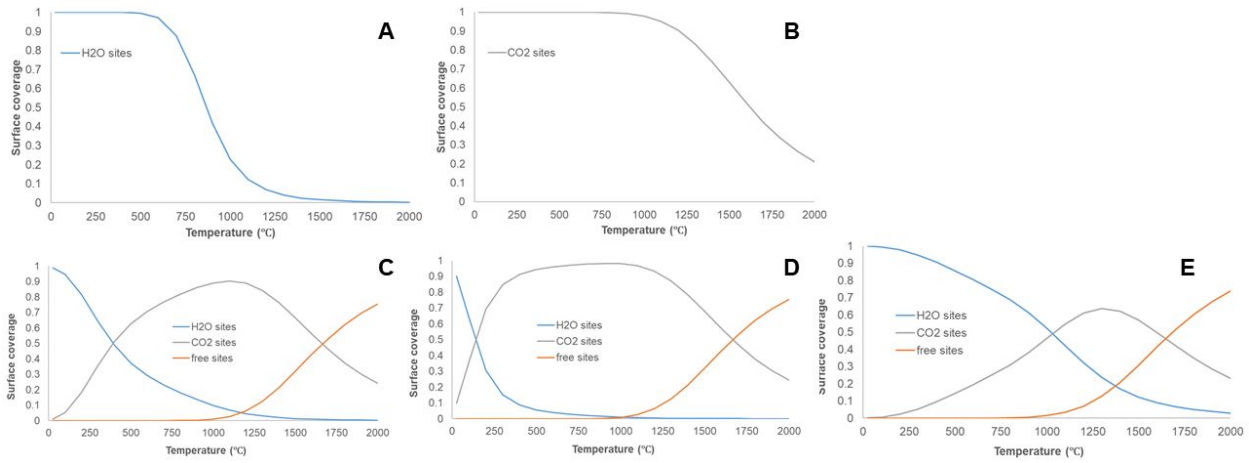


Figure 9. Surface coverage of CO_2 and H_2O. A: $P_{H2O}=10^{-5}$ in absence of CO_2; B: $P_{CO2}=3.9x10^{-4}$ in absence of H_2O; C: $P_{H2O}=10^{-5}$ and $P_{CO2}=3.9x10^{-4}$; D: $P_{H2O}=10^{-6}$ and $P_{CO2}=3.9x10^{-4}$; E: $P_{H2O}=10^{-4}$ and $P_{CO2}=3.9x10^{-4}$.

In Figure 9 A and B we investigated the surface coverage as a function of the temperature of H_2O and CO_2 respectively, in the absence of other co-adsorbing species. The P_{H2O} was set to 10^{-5} and the P_{CO2} was set to $3.9x10^{-4}$, e.g. concentration in air. Below 1000℃ the surface has full coverage of the adsorbing molecules and above 1000℃ the coverage gradually decreases to free surface oxide sites. In Figure 9 C we investigate the coadsorption of H_2O and CO_2 using equations 4 and 5. The P_{H2O} was set to 10^{-5} and the P_{CO2} was set to $3.9x10^{-4}$. In this simulation we assume that the surface is initially precovered with water. At low temperature the surface is completely covered with chemisorbed water. At 300℃ 35% of the surface sites are covered with carbonate. At 400℃ the surface is equally coved with chemisorbed water and carbonate. At 500℃ 62% of the surface is covered with carbonate. Above 500℃ the surface is dominated by the carbonate coverage reaching a peak of 90% at 1000℃. That result is consistent with recent measurements on thermal decomposition of $SrCO_3$.[40] At 1000℃ 3% of the surface consists of exposed free oxide sites. As the temperature increases the number of surface free sites increases and the carbonate coverage decreases. At 1600℃ the surface is characterized with 56% carbonate coverage, 42%free sites, and only 2% chemisorbed water. Above that temperature the surface is dominated by free sites, i.e. SrO termination. In Figure 9 D and E we investigate the effect of the water partial pressure by decreasing it to $P_{H2O}=10^{-6}$ and increasing it to $P_{H2O}=10^{-4}$, respectively. In case of $P_{H2O}=10^{-6}$ (Figure 9 D), at 300℃ 84% of the surface sites are covered with carbonate compared to 35% for $P_{H2O}=10^{-5}$. Above 300℃ the surface is dominated by the carbonate coverage reaching a peak of 98% at 1000℃. Above 1000℃ the behavior of the surface coverage doesn't depend significantly on the P_{H2O} as at that temperature most of the water is evacuated from the surface. In case of $P_{H2O}=10^{-4}$ (Figure 9 E), at 300℃ 5% of the surface sites are covered with carbonate compared to 35% for $P_{H2O}=10^{-5}$. At 1000℃ the surface is equally covered with chemisorbed water and carbonate. The carbonate coverage is reaching a peak of 63% at 1300℃. Above 1300℃ the behavior of the surface coverage doesn't depend significantly on the P_{H2O} as at that temperature most of the water is evacuated from the surface.

Conclusions

In this work we have investigated with theoretical and experimental techniques the interaction of O_2, CO_2, H_2O with SrO-terminated, $SrTiO_3$ surface. Our results have shown that the $SrTiO_3$ surface is dynamic and its structure, composition, and chemical reactivity, strongly depends on the environmental factors such as the chemical composition of the atmosphere to which the surface is exposed and the temperature. The SrO-terminated, $SrTiO_3$ surface reacts without activation barrier with both CO_2 and H_2O. As a result, either surface carbonate layer is formed or chemisorbed water with dissociated OH and H and strong surface hydrogen bonds. Thus, when exposed to dry air, the surface would be terminated with $SrCO_3$ precipitation. In the case of humidified air, the surface chemisorbed water molecules will be a natural barrier for carbonate formation. The reaction of the surface with CO_2 would be still possible but would require a significant activation barrier to replace the surface water. At low temperatures and humidified air the surface will be preferable terminated with chemisorbed water and with the increase of the temperature the water will be replaced by carbonate. At high temperature the carbonate will decompose to CO_2 and SrO-terminated surface. The surface composition will be a function of the temperature, P_{H2O}=10^{-5} and P_{CO2}.

The humidified air would have an additional positive effect for the surface oxygen exchange kinetics. In the case of SrO-terminated $SrTiO_3$, the rate constant for surface oxygen exchange reaction would increase 4 times at 800℃. This would be a result of a stabilized transition state geometry in the presence of water where a surface oxo-species would bind through a hydrogen bond to the water molecule. In the case of a dry air, that oxo species located over a Sr-Sr bridge would be highly unstable and characterized by a high activation barrier.

We should note that in this work we limit our research to several abundant molecules in the atmosphere: O_2, CO_2, and H_2O. However, depending on the geographical location, the atmospheric air may contain other molecules which can affect the surface composition, chemical properties and operation of devices with perovskite electrodes. Various NO_x and SO_x compounds can be found in the air close to sites with volcanic activity and large cities with thermal power plants and intensive automobile traffic and their effect on perovskite surfaces remain unclear.

Acknowledgements

A. S. acknowledges the support by KAKENHI grant number 18K05299. A. S., T. I., and J. K. acknowledge the support by World Premier International Research Center Initiative (WPI), Ministry of Education, Culture, Sports, Science, and Technology of Japan (MEXT), Japan, Solid Oxide Interfaces for Faster Ion Transport JSPS Core-to-Core Program (Advanced Research Networks), and the support from the JSPS, Japan and the NSF, US, under the JSPS-NSF Partnerships for International Research and Education (PIRE).

References:

1. Ishihara, T., *Structure and Properties of Perovskite Oxides. In: Ishihara T. (eds) Perovskite Oxide for Solid Oxide Fuel Cells. Fuel Cells and Hydrogen Energy.* Springer: Boston, MA 2009.
2. Kearney, K.; Iyer, A.; Rockett, A.; Staykov, A.; Ertekin, E., Effect of Surface Coverage and Composition on the Stability and Interfacial Dipole of Functionalized Silicon. *J. Phys. Chem. C* **2017,** *121*, 11312-11318.
3. Ida, S.; Kearney, K.; Futagami, T.; Hagiwara, H.; Sakai, T.; Watanabe, M.; Rockett, A.; Ishihara, T., Photoelectrochemical H2 evolution using TiO2-coated CaFe2O4 without an external applied bias under visible light irradiation at 470 nm based on device modeling. *Sus. En. Fuels* **2017,** *1*, 280-287.
4. Hagiwara, H.; Inoue, T.; Ida, S.; Ishihara, T., Long-time charge separation in porphyrin/KTa(Zr)O3 as water splitting photocatalyst. *Phys. Chem. Chem. Phys.* **2011,** *13*, 18031-18037.
5. Watanabe, M.; Hagiwara, H.; Ogata, Y.; Staykov, A.; Bishop, S. R.; Perry, N. H.; Chang, Y. J.; Ida, S.; Tanaka, K.; Ishihara, T., Impact of alkoxy chain length on carbazole-based, visible light-driven, dye sensitized photocatalytic hydrogen production. *J. Mater. Chem. A* **2015,** *3*, 21713-21721.
6. Watanabe, M.; Doi, Y.; Hagiwara, H.; Staykov, A. T.; Ida, S.; Matsumoto, T.; Shinmyozu, T.; Ishihara, T., Synthesis and Investigation of the Effect of Substitution on the Structure, Physical Properties, and Electrochemical Properties of Anthracenodifuran Derivatives. *J. Org. Chem.* **2015,** *80*, 9159-9166.

7. Watanabe, M.; Hagiwara, H.; Iribe, A.; Ogata, Y.; Shiomi, K.; Staykov, A.; Ida, S.; Tanaka, K.; Ishihara, T., Spacer effects in metal-free organic dyes for visible-light-driven dye-sensitized photocatalytic hydrogen production. *J. Mater. Chem. A* **2014,** *2*, 12952-12961.

8. Miyoshi, S.; Akbay, T.; Kurihara, T.; Fukuda, T.; Staykov, A. T.; Ida, S.; Ishihara, T., Fast Diffusivity of PF6– Anions in Graphitic Carbon for a Dual-Carbon Rechargeable Battery with Superior Rate Property. *J. Phys. Chem. C* **2016,** *120*, 22887-22894.

9. Skinner, S. J.; Kilner, J. A., Oxygen diffusion and surface exchange in La2−xSrxNiO4+δ. *Solid State Ionics* **2000,** *135*, 709-712.

10. Tarancon, A.; Skinner, S. J.; Chater, R. J.; Hernandez-Ramirez, F.; Kilner, J. A., Layered perovskites as promising cathodes for intermediate temperature solid oxide fuel cells. *J. Mater. Chem.* **2007,** *17*, 3175-3181.

11. Burriel, M.; Garcia, G.; Santiso, J.; Kilner, J. A.; Chater, R. J.; Skinner, S. J., Anisotropic oxygen diffusion properties in epitaxial thin films of La2NiO4+[small delta]. *J. Mater. Chem.* **2008,** *18*, 416-422.

12. Laguna-Bercero, M. A.; Kilner, J. A.; Skinner, S. J., Performance and Characterization of (La, Sr)MnO3/YSZ and La0.6Sr0.4Co0.2Fe0.8O3 Electrodes for Solid Oxide Electrolysis Cells. *Chem. Mater.* **2010,** *22*, 1134-1141.

13. Parfitt, D.; Chroneos, A.; Kilner, J. A.; Grimes, R. W., Molecular dynamics study of oxygen diffusion in Pr2NiO4+[small delta]. *Phys. Chem. Chem. Phys.* **2010,** *12*, 6834-6836.

14. Chroneos, A.; Yildiz, B.; Tarancon, A.; Parfitt, D.; Kilner, J. A., Oxygen diffusion in solid oxide fuel cell cathode and electrolyte materials: mechanistic insights from atomistic simulations. *En. Environm. Sci.* **2011,** *4*, 2774-2789.

15. Kushima, A.; Parfitt, D.; Chroneos, A.; Yildiz, B.; Kilner, J. A.; Grimes, R. W., Interstitialcy diffusion of oxygen in tetragonal La2CoO4+[small delta]. *Phys. Chem. Chem. Phys.* **2011,** *13*, 2242-2249.

16. Chen, Y.-C.; Yashima, M.; Peña-Martínez, J.; Kilner, J. A., Experimental Visualization of the Diffusional Pathway of Oxide Ions in a Layered Perovskite-type Cobaltite PrBaCo2O5+δ. *Chem. Mater.* **2013,** *25*, 2638-2641.

17. Goldschmidt, V. M., Die Gesetze der Krystallochemie. *Naturwissenschaften* **1926,** *14*, 477-485.

18. Wu, W.-Q.; Chen, D.; Caruso, R. A.; Cheng, Y.-B., Recent progress in hybrid perovskite solar cells based on n-type materials. *J. Mater. Chem. A* **2017,** *5*, 10092-10109.

19. Deacon-Smith, D. E. E.; Scanlon, D. O.; Catlow, C. R. A.; Sokol, A. A.; Woodley, S. M., Interlayer Cation Exchange Stabilizes Polar Perovskite Surfaces. *Adv. Mater.* **2014,** *26*, 7252-7256.

20. Staykov, A.; Tellez, H.; Druce, J.; Wu, J.; Ishihara, T.; Kilner, J., Electronic properties and surface reactivity of SrO-terminated SrTiO3 and SrO-terminated iron-doped SrTiO3. *Sci. Techn. Adv. Mater.* **2018,** *19*, 221-230.

21. Tasker, P. W., The stability of ionic crystal surfaces. *J. Phys. C: Solid State Phys.* **1979,** *12*, 4977.

22. Druce, J.; Tellez, H.; Burriel, M.; Sharp, M. D.; Fawcett, L. J.; Cook, S. N.; McPhail, D. S.; Ishihara, T.; Brongersma, H. H.; Kilner, J. A., Surface termination and subsurface restructuring of perovskite-based solid oxide electrode materials. *En. Environm. Sci.* **2014,** *7*, 3593-3599.

23. Staykov, A.; Téllez, H.; Akbay, T.; Druce, J.; Ishihara, T.; Kilner, J., Oxygen Activation and Dissociation on Transition Metal Free Perovskite Surfaces. *Chem. Mater.* **2015,** *27*, 8273-8281.

24. Akbay, T.; Staykov, A.; Druce, J.; Tellez, H.; Ishihara, T.; Kilner, J. A., The interaction of molecular oxygen on LaO terminated surfaces of La2NiO4. *J. Mater. Chem. A* **2016,** *4*, 13113-13124.

25. Sopiha, K. V.; Malyi, O. I.; Persson, C.; Wu, P., Band gap modulation of SrTiO3 upon CO2 adsorption. *Phys. Chem. Chem. Phys.* **2017,** *19*, 16629-16637.

26. Halwidl, D.; Mayr-Schmölzer, W.; Fobes, D.; Peng, J.; Mao, Z.; Schmid, M.; Mittendorfer, F.; Redinger, J.; Diebold, U., Ordered hydroxyls on Ca3Ru2O7(001). *Nature Comm.* **2017,** *8* (1), 23.

27. Li, M.; Sun, Z.; Yang, W.; Hong, T.; Zhu, Z.; Zhang, Y.; Wu, X.; Xia, C., Mechanism for the enhanced oxygen reduction reaction of La0.6Sr0.4Co0.2Fe0.8O3-[small delta] by strontium carbonate. *Phys. Chem. Chem. Phys.* **2017,** *19*, 503-509.

28. Kresse, G.; Furthmüller, J., Efficiency of ab-initio total energy calculations for metals and semiconductors using a plane-wave basis set. *Comp. Mater. Sci.* **1996,** *6*, 15-50.

29. Kresse, G.; Furthmüller, J., Efficient iterative schemes for ab initio total-energy calculations using a plane-wave basis set. *Phys. Rev. B* **1996,** *54*, 11169-11186.

30. Blöchl, P. E., Projector augmented-wave method. *Physical Review B* **1994,** *50* (24), 17953-17979.

31. Kresse, G.; Hafner, J., Ab initio. *Phys. Rev. B* **1993,** *47*, 558-561.

32. Das, T.; Nicholas, J. D.; Qi, Y., Long-range charge transfer and oxygen vacancy interactions in strontium ferrite. *J. Mater. Chem. A* **2017,** *5*, 4493-4506.

33. Piyanzina, I. I.; Kopp, T.; Yu, V. L.; Tayurskii, D. A.; Eyert, V., Electronic properties of LaAlO3/SrTiO 3 n-type interfaces: a GGA+ U study. *J. Phys.: Cond. Matt.* **2017,** *29*, 095501.

34. Momma, K.; Izumi, F., VESTA 3 for three-dimensional visualization of crystal, volumetric and morphology data. *J. Appl. Crystall.* **2011,** *44*, 1272-1276.

35. Halwidl, D.; Stoger, B.; Mayr-Schmolzer, W.; Pavelec, J.; Fobes, D.; Peng, J.; Mao, Z.; Parkinson, G. S.; Schmid, M.; Mittendorfer, F.; Redinger, J.; Diebold, U., Adsorption of water at the SrO surface of ruthenates. *Nat. Mater.* **2016,** *15*, 450-455.

36. Becerra-Toledo, A. E.; Enterkin, J. A.; Kienzle, D. M.; Marks, L. D., Water adsorption on SrTiO3(001): II. Water, water, everywhere. *Surf. Sci.* **2012,** *606*, 791-802.

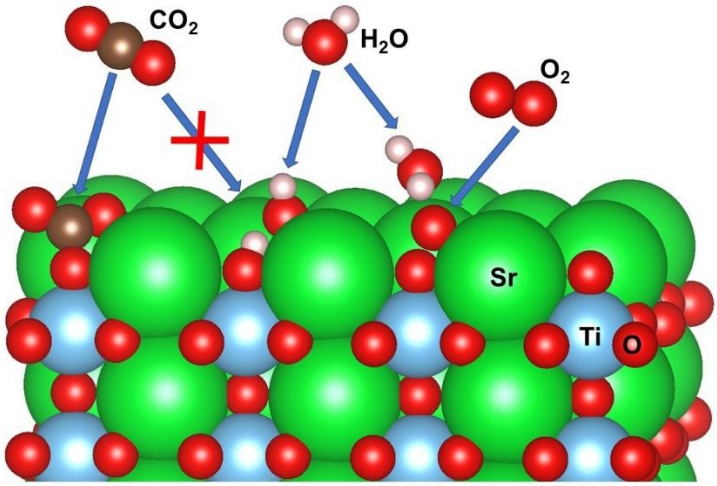
37. Evarestov, R. A.; Bandura, A. V.; Alexandrov, V. E., Adsorption of water on (001) surface of SrTiO3 and SrZrO3 cubic perovskites: Hybrid HF-DFT LCAO calculations. *Surf. Sci.* **2007,** *601*, 1844-1856.

38. Ishihara, T.; Fukui, S.; Matsumoto, H., Effects of Water Coexisting on the Cathode Activity for the Solid Oxide Fuel Cells Using LaGaO3-Based Perovskite Oxide Electrolyte. *J. Electrochem. Soc.* **2005,** *152,* A2035-A2039.

39. Gu, J.; Yan, Y.; Krizan, J. W.; Gibson, Q. D.; Detweiler, Z. M.; Cava, R. J.; Bocarsly, A. B., *p*-Type $CuRhO_2$ as a Self-Healing Photoelectrode for Water Reduction under Visible Light. *J. Am. Chem. Soc.*, **2014**, *136*, 830–833.

40. Ptáček, P.; Bartoníčková, E.; Švec, J.; Opravil, T.; Šoukal, F.; Frajkorová, F. The kinetics and mechanism of thermal decomposition of $SrCO_3$ polymorphs. *Ceramics Intern.*, **2015**, *41*, 115-126.

Table of content (TOC) graphics



Supplementary Information

Interaction of SrO-terminated $SrTiO_3$ Surface with Oxygen, Carbon Dioxide, and Water

Aleksandar Staykov,[a,*] Shun Fukumori,[b] Kazunari Yoshizawa,[b]
Kenta Sato,[c] Tatsumi Ishihara,[a,c] John Kilner[a,d]

[a)] International Institute for Carbon Neutral Energy Research, Kyushu University, Japan

[b)] Institute for Materials Chemistry and Engineering, Kyushu University, Japan

[c)] Applied Chemistry Department, Kyushu University, Japan

[d)] Materials Science Department, Imperial College London, UK

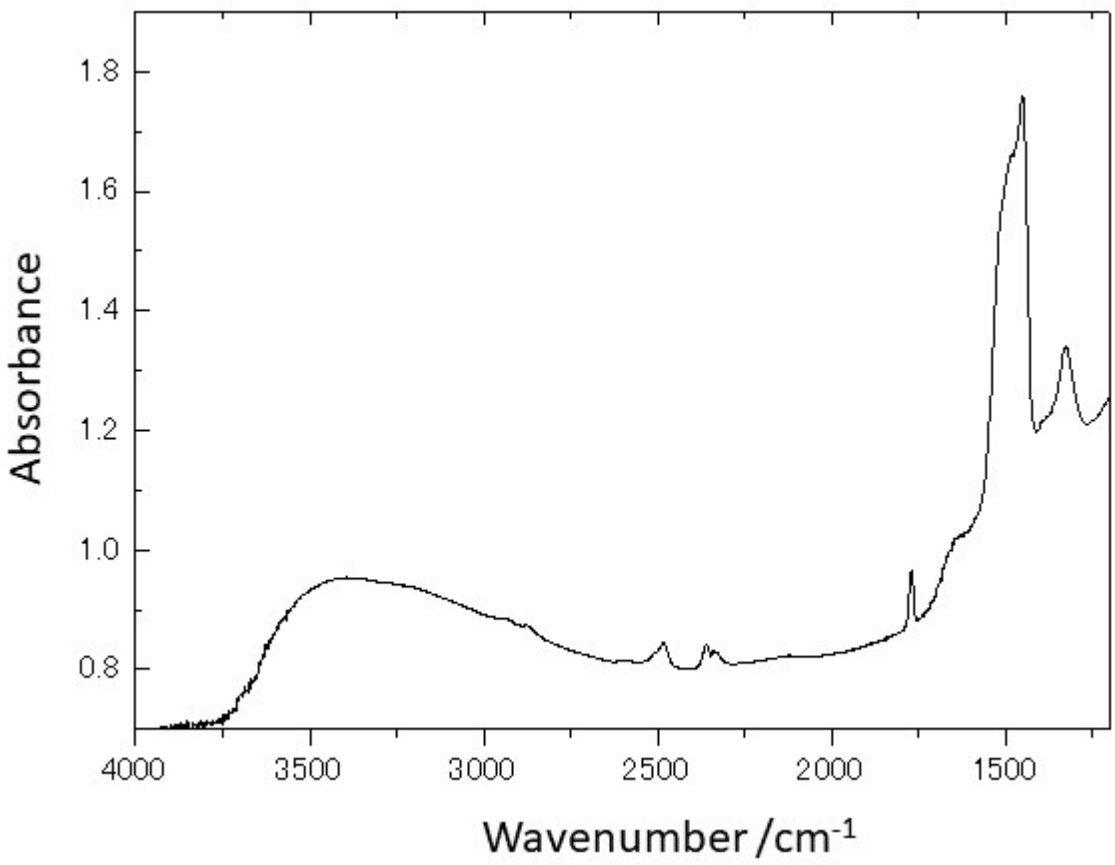


Figure S1: $SrTiO_3$ FTIR spectrum at 500°C after CO_2 and H_2O have been evacuated from the surface.